

Direct comparison of sterile neutrino constraints from cosmological data, ν_e disappearance data and $\nu_\mu \rightarrow \nu_e$ appearance data in a 3 + 1 model

Matthew Adams¹, Fedor Bezrukov¹, Jack Elvin-Poole², Justin J. Evans¹, Pawel Guzowski¹, Brian Ó Fearraigh^{3,4}, Stefan Söldner-Rembold¹

¹The University of Manchester, Department of Physics and Astronomy, Manchester, M13 9PL, United Kingdom

²Centre for Cosmology and Astro-Particle Physics, and Department of Physics, The Ohio State University, Columbus, OH 43210, USA

³Nikhef, National Institute for Subatomic Physics, PO Box 41882, Amsterdam, 1009 DB, The Netherlands

⁴University of Amsterdam, Institute of Physics/IHEF, PO Box 94216, Amsterdam, 1090 GE, The Netherlands

May 28, 2022

Abstract We present a quantitative, direct comparison of constraints on sterile neutrinos derived from neutrino oscillation experiments and from Planck data, interpreted assuming standard cosmological evolution. We extend a 1 + 1 model, which is used to compare exclusion contours at the 95% CL derived from Planck data to those from ν_e -disappearance measurements, to a 3 + 1 model. This allows us to compare the Planck constraints with those obtained through $\nu_\mu \rightarrow \nu_e$ appearance searches, which are sensitive to more than one active-sterile mixing angle. We find that the cosmological data fully exclude the allowed regions published by the LSND, MiniBooNE and Neutrino-4 collaborations, and those from the gallium and reactor anomalies, at the 95% CL. Compared to the exclusion regions from the Daya Bay ν_e -disappearance search, the Planck data are more strongly excluding above $|\Delta m_{41}^2| \approx 0.1 \text{ eV}^2$ and $m_{\text{eff}}^{\text{sterile}} \approx 0.2 \text{ eV}$, with the Daya Bay exclusion being stronger below these values. Compared to the combined Daya Bay/Bugey/MINOS exclusion region on $\nu_\mu \rightarrow \nu_e$ appearance, the Planck data is more strongly excluding above $\Delta m_{41}^2 \approx 5 \times 10^{-2} \text{ eV}^2$, with the exclusion strengths of the Planck data and the Daya Bay/Bugey/MINOS combination becoming comparable below this value.

1 Introduction

The LSND [1], MiniBooNE [2], and Neutrino-4 [3] collaborations have made observations consistent with anomalous neutrino flavour oscillations. Other, related anomalies have been measured with gallium detectors [4] and reactor neutrinos [5]. These observations suggest that additional neutrino flavours may exist at a mass scale of $O(1 \text{ eV})$, beyond the three flavours of the Standard Model.

Measurements of the decay width of the Z boson [6] conclusively show that only three neutrino flavours with

$m_\nu < m_Z/2$ couple through the weak interaction; these three flavours are termed “active”, and any additional flavours are therefore referred to as “sterile”. The existence of a sterile neutrino can have observable effects since neutrino oscillations allow the sterile flavour states to mix with the active flavour states. Such mixing occurs as the neutrino mass eigenstates are related to the flavour eigenstates through a mixing matrix, the PMNS matrix [7–9]. The minimal phenomenological 3 + 1 model of sterile neutrinos adds a single sterile flavour state and a fourth mass eigenstate.

Limits on the existence of sterile neutrinos have been set by observations of the cosmic microwave background (CMB) [10] and by numerous neutrino oscillation experiments [11–17]. In a commonly used model, cosmological measurements set limits on the parameter ΔN_{eff} , the additional number of relativistic degrees of freedom in the universe arising from the additional neutrino states, and $m_{\text{eff}}^{\text{sterile}}$, the effective mass of the sterile neutrino. In a 3+1 model, neutrino oscillation experiments set limits on the mass splitting $\Delta m_{41}^2 = m_4^2 - m_1^2$, the difference between the squared masses of the additional, fourth mass eigenstate and the lightest neutrino eigenstate, along with the elements of the 4×4 PMNS matrix.

Quantitative comparisons of cosmological and neutrino-oscillation limits on sterile neutrinos are complicated due to this difference in parameterization. In a previous article [18], a comparison using a phenomenological model in which only the muon-neutrino flavour mixes into the fourth mass eigenstate was presented. This 1 + 1 model allows only comparisons of ν_μ disappearance measurements to the cosmological limits. Other studies [19] have investigated the situation in which only the electron-neutrino flavour is assumed to mix into the fourth mass eigenstate. In this article, we extend our treatment to the full 3 + 1 model, allowing us to compare the cosmological limits to both ν_e and $\bar{\nu}_e$ disappearance measurements, including the gallium and reactor

anomalies, and to the LSND and MiniBooNE $\bar{\nu}_\mu \rightarrow \bar{\nu}_e$ and $\nu_\mu \rightarrow \nu_e$ observations. In addition, we develop a treatment that allows us to extend our comparisons into the so-called degenerate region in which the sterile mass-splitting Δm_{41}^2 becomes equal to the mass splitting Δm_{31}^2 .

2 Sterile neutrinos in oscillation experiments

In the 3 + 1 model, four neutrino flavour eigenstates, ν_l ($l = e, \mu, \tau, s$), are related to four neutrino mass eigenstates, ν_i ($i = 1, 2, 3, 4$), with masses m_i , by a 4×4 extension of the PMNS matrix, U :

$$|\nu_l\rangle = \sum_{i=1}^4 U_{li} |\nu_i\rangle. \quad (1)$$

Throughout this paper, we assume all neutrino and antineutrino oscillation probabilities are equal and therefore use the symbol ν to also refer to $\bar{\nu}$. If a neutrino of energy E is produced in a flavour eigenstate ν_l , the probability that it is detected in flavour eigenstate $\nu_{l'}$ after traveling a distance L is

$$P_{\nu_l \rightarrow \nu_{l'}} = \left| \sum_{i=1}^4 U_{li} U_{l'i}^* e^{-im_i^2 L/2E} \right|^2. \quad (2)$$

An experiment searching for ν_e or ν_μ disappearance thus measures

$$1 - P_{\nu_l \rightarrow \nu_l} = 4 \sum_{i=1}^3 \sum_{j>i}^4 |U_{li}|^2 |U_{lj}|^2 \sin^2 \left(\frac{\Delta m_{ji}^2 L}{4E} \right), \quad (3)$$

where $\Delta m_{ji}^2 = m_j^2 - m_i^2$ are the mass splittings. Each mass splitting therefore defines an observable oscillation wavelength, with the elements of the PMNS matrix governing the amplitudes of those oscillations.

Over the majority of the parameter space relevant to sterile-neutrino searches, $|\Delta m_{41}^2| \gg |\Delta m_{31}^2| > |\Delta m_{21}^2|$. Thus, we can choose L and E to probe only the oscillations at the Δm_{41}^2 wavelength, allowing us to approximate the disappearance probabilities in Eq. 3 to

$$1 - P_{\nu_e \rightarrow \nu_e} \approx \sin^2(2\theta_{14}) \sin^2 \left(\frac{\Delta m_{41}^2 L}{4E} \right), \quad (4)$$

$$1 - P_{\nu_\mu \rightarrow \nu_\mu} \approx \sin^2(2\theta_{24}) \sin^2 \left(\frac{\Delta m_{41}^2 L}{4E} \right). \quad (5)$$

Here, we have introduced the mixing angles θ_{ij} that are used to parameterize the PMNS matrix. We refer to this approximation of the oscillation probabilities as a 1 + 1 model since it assumes only one mass splitting, neglecting the effects of Δm_{31}^2 and Δm_{21}^2 , and assuming only one flavour state at a time (either electron or muon) mixes into the fourth mass eigenstate. The mixing angle θ_{14} quantifies how much electron

flavour mixes into the fourth mass eigenstate, and the angle θ_{24} quantifies this mixing for the muon flavour. In this paper, we use the 1 + 1 model for an analysis of ν_e disappearance.

In our analysis of $\nu_\mu \rightarrow \nu_e$ appearance we use a 3 + 1 model, in which there are three independent mass splittings (Δm_{21}^2 , Δm_{31}^2 and Δm_{41}^2), six mixing angles (θ_{12} , θ_{13} , θ_{23} , θ_{14} , θ_{24} , and θ_{34}), and three complex phases (δ_{13} , δ_{14} and δ_{34}). Still, only the angles θ_{14} and θ_{24} and the mass-splitting Δm_{41}^2 are relevant to this work. We set $\theta_{34} = \delta_{14} = \delta_{34} = 0$, as these parameters have no impact on our results. The remaining oscillation parameters we set to the best-fit values from a global fit [20], assuming normal mass ordering: $\Delta m_{21}^2 = 7.50 \times 10^{-5} \text{ eV}^2$, $\Delta m_{31}^2 = 2.524 \times 10^{-3} \text{ eV}^2$, $\sin^2 \theta_{12} = 0.306$, $\sin^2 \theta_{13} = 0.02166$, $\sin^2 \theta_{23} = 0.441$, and $\delta_{13} = 0$.

We use the exact oscillation formula for our analysis of ν_e appearance. Since in the region of large Δm_{41}^2 the relevant oscillation probability for $\nu_\mu \rightarrow \nu_e$ is, to a good approximation,

$$P_{\nu_\mu \rightarrow \nu_e} \approx \sin^2(2\theta_{14}) \sin^2 \theta_{24} \sin^2 \left(\frac{\Delta m_{41}^2 L}{4E} \right), \quad (6)$$

we express limits as a function of Δm_{41}^2 and $\sin^2(2\theta_{14}) \sin^2 \theta_{24} \equiv \sin^2(2\theta_{\mu e})$.

3 Data from oscillation experiments

We use data from collaborations that report allowed regions consistent with sterile neutrino oscillations. Such regions have been reported by the LSND, MiniBooNE, and Neutrino-4 collaborations, in addition to the regions allowed by the reactor and gallium anomalies. We then compare to the exclusion region from Daya Bay, combined with Bugey-3 and MINOS data, which provides stronger exclusion at lower values of the mass of the fourth mass eigenstate, where the sensitivity of the Planck results decreases.

3.1 LSND

The Liquid Scintillator Neutrino Detector (LSND) took data from 1993–1998 at the Los Alamos Meson Physics Facility. A 167 t liquid scintillator detector was placed 30 m away from a stopped-pion source that produced $\bar{\nu}_\mu$ with energies up to 52.8 MeV [21]. Appearance of $\bar{\nu}_e$ was observed in the detector with a total excess of $87.9 \pm 22.4(\text{stat.}) \pm 6.0(\text{syst.})$ $\bar{\nu}_e$ events above the expected background [1]. To explain this excess through oscillations, a mass splitting $\Delta m_{41}^2 \gtrsim 0.03 \text{ eV}^2$ is required.

We determine the 90% Confidence Level (CL) allowed region by requiring $\chi^2 - \chi_{\min}^2 = 4.605$ between the observed positron energy spectrum and an estimated spectrum. The appearance spectrum is simulated with pseudo-experiments,

producing a reconstructed neutrino energy from a reconstructed positron energy and angle, and integrating the reconstructed neutrino energy over the same binning as in Ref. [1]. The true positron energy, E_{e^+} , is the difference between the true neutrino energy and the threshold energy of 1.806 MeV. The $\bar{\nu}_e \rightarrow e^+$ cross section is estimated to be linear in E_{e^+} . The reconstructed positron energy is smeared by a Gaussian function of the form $7\%/\sqrt{E_{e^+}/52.8 \text{ MeV}}$, and its angle is Gaussian-smeared by 12° . The distance L that the neutrino has travelled is uniformly spread in the range [25.85, 34.15] m, and a 14 cm Gaussian smearing is applied to produce a reconstructed distance. The flux is determined for pions decaying at rest to $\bar{\nu}_\mu$, with an L^{-2} weighting applied. The true neutrino energy and distance is used to calculate the oscillated $\bar{\nu}_e$ flux with Eq. 6.

3.2 MiniBooNE

The MiniBooNE experiment was an 818 t mineral oil Cherenkov detector [22] 541 m away from the neutrino-production target of the Booster Neutrino Beam [23]. The beam could be configured to produce either ν_μ or $\bar{\nu}_\mu$ with mean energy of ≈ 800 MeV. By searching for the appearance of either ν_e or $\bar{\nu}_e$, the experiment was sensitive to oscillations driven by a similar range of Δm_{41}^2 as LSND. An excess of activity consistent with ν_e and $\bar{\nu}_e$ was observed. We use the CL contours from the Collaboration's public data release [24].

3.3 Neutrino-4

The Neutrino-4 experiment [3] searches for the disappearance of $\bar{\nu}_e$ from the SM3 reactor in Russia. A gadolinium-doped liquid scintillator detector is divided into 50 sections that can be placed at various distances, from 6 to 12 m, from the reactor core. The data analysis yields an oscillatory pattern to the $\bar{\nu}_e$ detection rate as a function of L/E that is interpreted in terms of a sterile neutrino with best-fit oscillation parameters $\Delta m_{41}^2 = 7.34 \text{ eV}^2$, $\sin^2(2\theta_{14}) = 0.44$. We take the 95% CL allowed region directly from Ref. [3].

3.4 Reactor anomaly

The reactor anomaly, first described in Ref. [5], is the observation that, with more modern flux calculations, many short-baseline reactor- $\bar{\nu}_e$ searches show a deficit compared to the expected flux. This observation can be interpreted as $\bar{\nu}_e$ disappearance due to oscillations involving a sterile neutrino. We use the 95% CL allowed region calculated in Ref. [25].

3.5 Gallium anomaly

The gallium anomaly, first described in Ref. [4], measured the ν_e rate from radioactive calibration sources in the SAGE and GALLEX solar-neutrino detectors. A deficit in the measured rate compared to the expectation can be interpreted as ν_e disappearance due to oscillations involving a sterile neutrino. We use the 95% CL allowed region calculated in Ref. [25].

3.6 Daya Bay

The Daya Bay experiment consists of eight gadolinium-doped liquid scintillator detectors that measure the disappearance of electron antineutrinos from the Daya Bay and Ling Ao nuclear power plants in China [26]. The arrangement of eight detectors and six reactor cores provides a range of baselines between 358 m and 1925 m. The Daya Bay experiment was designed to be sensitive to oscillations driven by Δm_{31}^2 and θ_{13} [27]; however, by looking for non-standard $\bar{\nu}_e$ disappearance, Daya Bay can also search for oscillations driven by Δm_{41}^2 and θ_{14} in the range $10^{-4} \lesssim |\Delta m_{41}^2| \lesssim 0.1 \text{ eV}^2$ [13]. We use the Daya Bay data release [28] to recreate the χ^2 surface, and follow the prescribed approach [29], based on the CL_s method [30, 31], to produce the 95% CL exclusion contour.

3.7 Bugey-3

The Bugey-3 experiment took data in the early 1990s. The experiment used two lithium-doped liquid-scintillator detectors [32] to search for the disappearance of $\bar{\nu}_e$ at distances of 15 m, 40 m and 95 m from the Bugey nuclear power plant in France [33]. The shorter baseline provides sensitivity to sterile neutrinos at a higher range of $|\Delta m_{41}^2|$ compared to Daya Bay.

3.8 MINOS

The MINOS experiment used two steel-scintillator calorimeters [34] to search for the disappearance of muon neutrinos and antineutrinos from the NuMI beam at Fermilab [35] at baselines of 1.04 km and 735 km. MINOS was designed to be sensitive to oscillations driven by Δm_{31}^2 and θ_{23} [36]. By searching for non-standard ν_μ and $\bar{\nu}_\mu$ disappearance at higher energies, it is also sensitive to oscillations driven by the sterile-neutrino parameters Δm_{41}^2 and θ_{24} [11].

3.9 Combination of Daya Bay, Bugey-3, and MINOS Data

The Daya Bay limit was combined with that of Bugey-3 and MINOS to produce limits on the parameters Δm_{41}^2 and

$\sin^2(2\theta_{\mu e})$ that govern $\nu_\mu \rightarrow \nu_e$ appearance [14]. In performing this combination, the analysis of the Bugey-3 data was updated to use a more recent calculation of the neutron lifetime in the cross-section of the inverse- β decay process that is used for $\bar{\nu}_e$ detection. In addition, the ILL+Vogel flux model [37, 38] was replaced with the Huber-Mueller model [39, 40]. We use the combined CL_s surface of Ref. [41] to reproduce the 95% CL exclusion contour.

4 Sterile neutrinos in cosmological measurements

The presence of one or more sterile neutrinos can affect the power spectrum of the CMB. The effective mass of the sterile neutrino is defined as $m_{\text{eff}}^{\text{sterile}} = (94.1 \Omega_{\text{sterile}} h^2) \text{ eV}$, where $h = H/100$ with the Hubble parameter H , and Ω_{sterile} is the contribution of sterile neutrinos to the matter energy-density in the Universe. The neutrino number density, n_ν , is expressed as a function of the number of effective neutrino species, N_{eff} , as

$$n_\nu = \left(\frac{3}{4}\right) N_{\text{eff}} \left(\frac{4}{11}\right) n_\gamma, \quad (7)$$

where n_γ is the number density of photons in the CMB. Standard cosmology predicts $N_{\text{eff}} = 3.046$, since the process of neutrino decoupling from the CMB was not instantaneous, and neutrinos still interacted with leptons in the primordial plasma [42]. This allows us to define the effective number of additional radiative degrees of freedom, equivalent to the effective number of additional neutrino species, as $\Delta N_{\text{eff}} = N_{\text{eff}} - 3.046$.

We relate $m_{\text{eff}}^{\text{sterile}}$ and the mass of the fourth neutrino mass eigenstate, m_4 using the standard relationship [10]

$$m_{\text{eff}}^{\text{sterile}} = \left(\frac{T_s}{T_\nu}\right)^3 m_4 = (\Delta N_{\text{eff}})^{3/4} m_4. \quad (8)$$

Here, we assume a thermally distributed sterile neutrino with a temperature T_s that may differ from the active neutrino thermalisation temperature T_ν .

A fully thermalized sterile neutrino with temperature $T_s = T_\nu$ corresponds to a measured $\Delta N_{\text{eff}} = 1$ and $m_{\text{eff}}^{\text{sterile}} = m_4$. An alternative relationship between $m_{\text{eff}}^{\text{sterile}}$ and m_4 , the Dodelson-Widrow mechanism [43], assumes that ΔN_{eff} acts as a linear scaling factor, $m_{\text{eff}}^{\text{sterile}} = \Delta N_{\text{eff}} m_4$. The choice of this function does not significantly impact our results.

5 The Planck experiment

The Planck satellite made detailed observations of anisotropies of the CMB between 2009 and 2013, over a frequency range from 30 to 857 GHz [44, 45]. The Planck Collaboration combines data from the TT, TE and EE power spectra, the

low-multipole EE power spectrum (LowE), CMB lensing, and baryon acoustic oscillations (BAO) to set limits of $N_{\text{eff}} < 3.29$ and $m_{\text{eff}}^{\text{sterile}} < 0.23 \text{ eV}$ [10]. These results arise from the use of a flat prior in the range $0 < m_{\text{eff}}^{\text{sterile}} < 10 \text{ eV}$. A more restrictive prior results in more constraining limits. A flat prior in the range $0 < \Delta N_{\text{eff}} < 1$ is also used. The Planck analysis assumes a normal neutrino-mass ordering and active states with masses $m_1 = m_2 = 0$ and $m_3 = 0.06 \text{ eV}$.

To obtain these limits on sterile neutrinos, the Planck Collaboration fits the data using a $\Lambda\text{CDM} + m_{\text{eff}}^{\text{sterile}} + \Delta N_{\text{eff}}$ model, varying neutrino and nuisance parameters to build a large number of points in the parameter space. The number density of these points is proportional to the probability density. We produce exclusion limits in the $(\Delta N_{\text{eff}}, m_{\text{eff}}^{\text{sterile}})$ space by integrating over 95% of the probability density relative to the maximum value, using the Markov chain Monte Carlo data released by the Planck collaboration [10, 46].

6 Electron neutrino disappearance in a 1 + 1 model

To translate from the parameter space $(\Delta N_{\text{eff}}, m_{\text{eff}}^{\text{sterile}})$ to the parameter space $(\sin^2 2\theta_{14}, |\Delta m_{41}^2|)$, we use LASAGNA [47] for calculating ΔN_{eff} as a function of the mass splitting $|\Delta m_{41}^2|$ and mixing angle $\sin^2 2\theta_{14}$. LASAGNA solves the quantum kinetic equations describing neutrino thermalization in the early universe by evolving the equations over a temperature range for input values of $|\Delta m_{41}^2|$ and $\sin^2(2\theta_{14})$.

Limits from neutrino disappearance experiments can be interpreted in the 1 + 1 model, which assumes that only one active flavour state mixes into the fourth mass state and that the three other mass states form a single, mass-degenerate state, ν_d . For ν_e disappearance experiments, we allow only the ν_e flavour to mix into the fourth mass state. This is equivalent to varying θ_{14} whilst fixing $\theta_{24} = \theta_{34} = 0$. In this model, we can write

$$\nu_e = \cos \theta_{14} \nu_d - \sin \theta_{14} \nu_4, \quad (9)$$

$$\nu_s = \sin \theta_{14} \nu_d + \cos \theta_{14} \nu_4. \quad (10)$$

LASAGNA calculates the Bloch vectors

$$(P_0, \mathbf{P}) = (P_0, P_x, P_y, P_z) \quad (11)$$

for neutrinos and $(\bar{P}_0, \bar{\mathbf{P}})$ for anti-neutrinos using the 1 + 1 model. The resulting vector $P_s^+ = (P_0 + \bar{P}_0) + (P_x + \bar{P}_x)$ enters the expression

$$\Delta N_{\text{eff}} = \frac{\int (p/T)^3 (1 + e^{p/T})^{-1} P_s^+ d(\frac{p}{T})}{4 \int (p/T)^3 (1 + e^{p/T})^{-1} d(\frac{p}{T})}, \quad (12)$$

where the momentum distribution, p , of the neutrinos is assumed to obey a Fermi-Dirac distribution at temperature T . A temperature range of $T = [40, 1] \text{ MeV}$ covers the period from the beginning to the end of decoupling. We assume the lepton asymmetry, $L = (n_l - n_{\bar{l}})/n_\gamma$, to be zero. It was shown

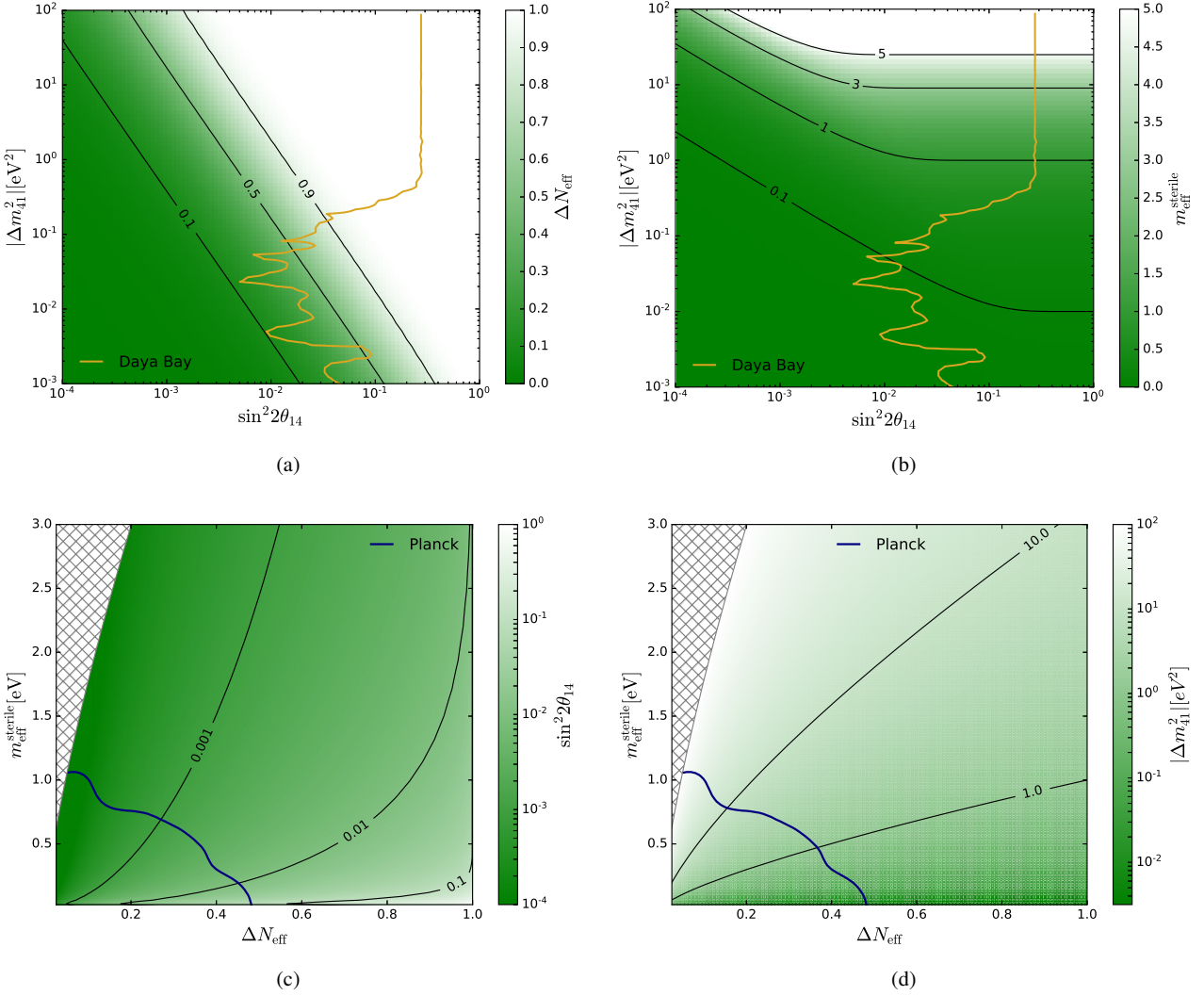


Fig. 1 (a, b) Cosmological parameters $\Delta N_{\text{eff}}^{\text{sterile}}$ and $m_{\text{eff}}^{\text{sterile}}$ calculated, using LASAGNA, in the oscillation space of the 1 + 1 model that is relevant for ν_e and $\bar{\nu}_e$ disappearance measurements. We use the thermal sterile neutrino mass (Eq. 8) and assume vanishing lepton asymmetry ($L = 0$). We also show the Daya Bay exclusion contour; the region to the right of the contour is ruled out at the 95% CL. (c, d) The oscillation parameters of the 1 + 1 electron-neutrino disappearance model, Δm_{41}^2 and $\sin^2(2\theta_{14})$, in the cosmological space ($m_{\text{eff}}^{\text{sterile}}$, ΔN_{eff}). The region above the blue line is excluded by the Planck TT, TE, EE and low-multipole EE power spectra at the 95% CL. A prior of $m_4 < 10$ eV is applied, shown by the hatched region that has not been considered in our probability density estimation.

in Ref. [18] that the Planck exclusion region is significantly reduced in a 1+1 model for ν_μ disappearance for large lepton asymmetries ($L = 10^{-2}$).

We use LASAGNA to calculate ΔN_{eff} for a grid in the oscillation parameter space of $|\Delta m_{41}^2| \equiv |m_4^2 - m_d^2|$ and $\sin^2(2\theta_{14})$, as shown in Fig. 1(a). Equation 8 allows us to express this result for all relevant combinations of ΔN_{eff} , $m_{\text{eff}}^{\text{sterile}}$, $\sin^2(2\theta_{14})$, and $|\Delta m_{41}^2|$ (Figs. 1(b)–1(d)).

In Fig. 2(a) we express the Planck exclusion limit in the parameter space ($\sin^2(2\theta_{14})$, $|\Delta m_{41}^2|$) and overlay the limit from Daya Bay, and the allowed regions from Neutrino-4 and the gallium and reactor anomalies. The equivalent contours translated into the cosmological parameter space

($m_{\text{eff}}^{\text{sterile}}$, ΔN_{eff}) are shown in Fig. 2(b). In both figures, we show the Planck limit with and without the BAO and CMB lensing data.

The limits obtained using the Planck data with and without the BAO and CMB lensing data are strongly constraining in both parameter spaces in the region above $|\Delta m_{41}^2|^2 \approx 0.1$ eV² and $m_{\text{eff}}^{\text{sterile}} \approx 0.2$ eV, and exclude the allowed regions from the Neutrino-4 experiment, and from the gallium and reactor anomalies. The Daya Bay experiment is sensitive to the regions of low $|\Delta m_{41}^2|$ and $m_{\text{eff}}^{\text{sterile}}$, where the cosmological data are less constraining.

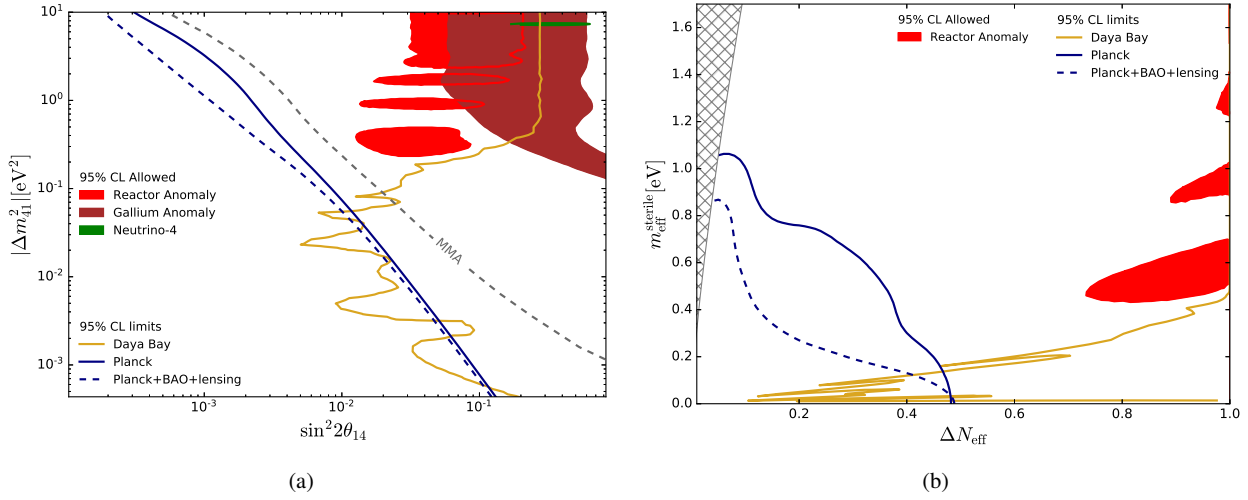


Fig. 2 (a) shows, in the neutrino-oscillation parameter space, limits on the electron flavour mixing with the fourth mass state, using a 1 + 1 model. The exclusion region from the Daya Bay oscillation experiment, and the allowed regions from the Neutrino-4 experiment and the reactor anomaly, come from searches for $\bar{\nu}_e$ disappearance. The allowed region from the gallium anomaly comes from a search for ν_e disappearance. For the Daya Bay line, everything to the right is ruled out at 95% CL. The solid blue line labeled ‘Planck’ shows the exclusion using the Planck TT, TE, EE and low-multipole EE power spectra, using Eq. 8 to relate $m_{\text{eff}}^{\text{sterile}}$ to m_4 , with the region to the right ruled out at 95% CL. The dashed blue line shows the impact of further including CMB and BAO data into the Planck limit, again using Eq. 8. The dashed grey line illustrates the impact on the Planck limit (the solid blue) of using the mean momentum approximation (MMA). Graph (b) shows the same set of limits (minus the MMA line) in the cosmological parameter space. The Neutrino-4 and gallium-anomaly lines are no longer visible as they are compressed up along the $\Delta N_{\text{eff}} = 1$ axis. The hatched region corresponds to the prior of $m_4 < 10$ eV assumed in the Planck analysis.

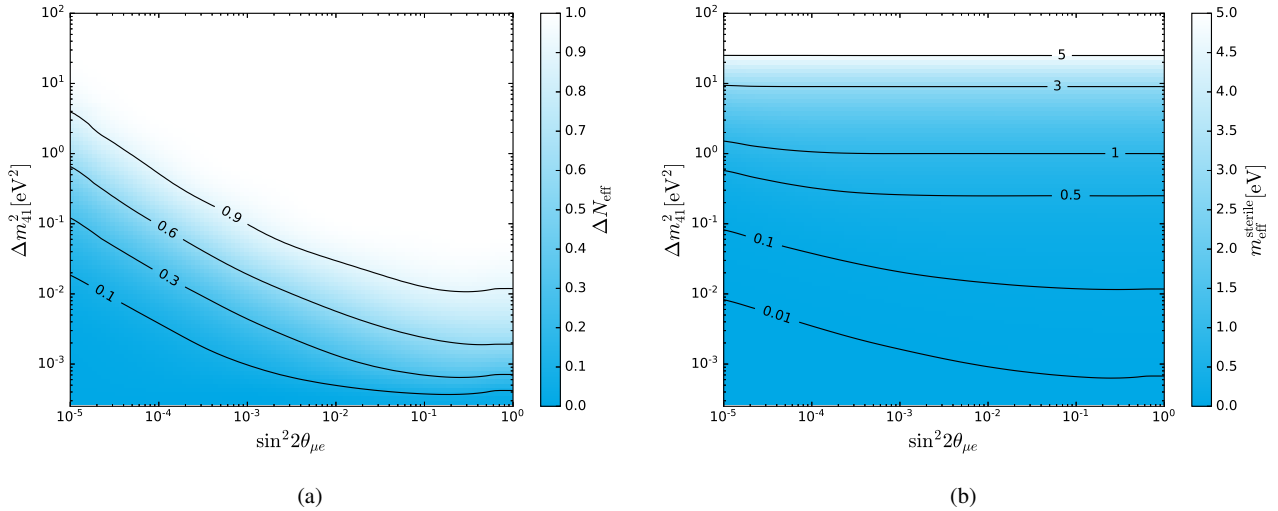


Fig. 3 The cosmological parameters (a) ΔN_{eff} and (b) $m_{\text{eff}}^{\text{sterile}}$ calculated in the oscillation parameter space (Δm_{41}^2 , $\sin^2(2\theta_{\mu e})$) using the mean momentum approximation as described in the text.

7 Electron neutrino appearance in a 3 + 1 model

When considering $\sin^2(2\theta_{\mu e})$, both mixing angles θ_{14} and θ_{24} must be allowed to be non-zero to allow both ν_e and ν_μ flavours to mix into the ν_4 state, and so we work in the 3 + 1 model with one sterile and three active neutrino flavours, albeit setting $\theta_{34} = 0$. This model can be solved exactly [48] but working with the full momentum dependence of the

quantum kinetic equations is computationally very intensive. Hence, we use the mean momentum approximation (MMA) following the prescription of Ref. [49] summarized below.

The neutrino density matrix,

$$\rho(x, y) = \begin{pmatrix} \rho_{ee} & \rho_{e\mu} & \rho_{e\tau} & \rho_{es} \\ \rho_{\mu e} & \rho_{\mu\mu} & \rho_{\mu\tau} & \rho_{\mu s} \\ \rho_{\tau e} & \rho_{\tau\mu} & \rho_{\tau\tau} & \rho_{\tau s} \\ \rho_{se} & \rho_{s\mu} & \rho_{s\tau} & \rho_{ss} \end{pmatrix}, \quad (13)$$

depends on the mixing angles and mass splittings. It can be written as a function of reduced time, $x \equiv m/T$, and reduced momentum, $y \equiv p/T$, where m is an arbitrary mass scale and T is the initial temperature of the thermal, active neutrinos. This matrix is used to calculate ΔN_{eff} for any required values of θ_{14} , θ_{24} and Δm_{41}^2 as

$$\Delta N_{\text{eff}} = \frac{1}{2} (\text{Tr}(\rho) + \text{Tr}(\bar{\rho}) - 6). \quad (14)$$

The MMA assumes that the momentum dependence of $\rho(x, y)$ can be factorized out as a Fermi-Dirac distribution, $\rho(x, y) \rightarrow f_{\text{FD}}(y)\rho(x)$. The equations of motion for the neutrino and anti-neutrino density matrices is then written assuming that all neutrinos have the same momentum, $\langle y \rangle$.

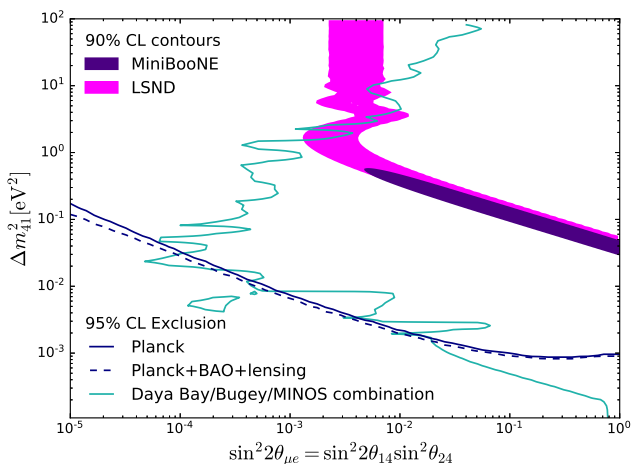


Fig. 4 Limits on the parameters governing $\nu_{\mu} \rightarrow \nu_e$ appearance in a 3+1 model, shown in the neutrino-oscillation parameter space. Solid regions are the allowed regions from the MiniBooNE and LSND measurements. The light blue line is an exclusion region from the Daya Bay/Bugey/MINOS combined analysis. The dark blue lines show the Planck exclusion region, expressed in this parameter space, with (dashed) and without (solid) the BAO and CMB lensing data included.

We solve the resulting differential equations of motion numerically with an implicit Runge-Kutta algorithm of order 5, RADAU5 [50], using a publicly available C++ implementation [51]. To evaluate ΔN_{eff} , we evolve the density matrix from $T = 100$ MeV to $T = 1$ MeV. To project the cosmological limits onto the $\sin^2(2\theta_{\mu e})$ axis, we minimise the value of ΔN_{eff} as a function of θ_{14} and θ_{24} along a contour of constant $\sin^2(2\theta_{\mu e})$; the derived 95% confidence limits therefore assume the maximum possible thermalisation for a given value of $\theta_{\mu e}$. The resulting values of ΔN_{eff} as a function of Δm_{41}^2 and $\sin^2(2\theta_{\mu e})$ are shown in Fig 3.

In the region $|\Delta m_{41}^2| \lesssim |\Delta m_{31}^2|$, the mass splitting Δm_{41}^2 is driving neutrino oscillations at wavelengths similar to those driven by the active-neutrino mass splittings. This is referred to as the degenerate region, and in this region the RADAU5

solver slows down drastically due to the stiffness of the problem when degeneracies are crossed. To mitigate this, we increase the tolerance by a factor of 10 after every 100,000 steps of the algorithm, starting from a default tolerance of 10^{-10} , reaching a maximum tolerance of 10^{-4} required for certain parameters to converge quickly.

We evaluate the impact of the MMA by repeating the ν_e disappearance analysis in the 1 + 1 model using this approximation. The result of this is shown in Fig 2(a), illustrating that, under the MMA, the cosmological exclusion contours expressed in the $(\Delta m_{41}^2, \sin^2(2\theta_{14}))$ parameter space become slightly weaker.

In Figure 4, we show the Planck exclusion contours, with and without the BAO and CMB lensing data, in the $(\Delta m_{41}^2, \sin^2(2\theta_{\mu e}))$ parameter space. We compare this to the limits from the Daya Bay/Bugey/MINOS combination, and the allowed regions from the LSND and MiniBooNE $\nu_e \rightarrow \nu_{\mu}$ searches. The Planck exclusion region strongly excludes the entirety of the LSND and MiniBooNE allowed regions. The Daya Bay/Bugey/MINOS combined exclusion region is comparable in its exclusion power to that from the Planck data for mass splittings below $\Delta m_{41}^2 \approx 5 \times 10^{-2}$ eV² and becomes more constraining below $\Delta m_{41}^2 \approx 10^{-3}$ eV².

8 Conclusions

The discovery of a sterile neutrino would have major implications for the field of particle physics. The presence of both possible observations from neutrino oscillation experiments such as LSND and MiniBooNE, negative results from other oscillation experiments, and negative results from cosmological experiments, have left the field in an ambiguous situation. A particular challenge in drawing conclusions is quantitative comparison of limits from neutrino oscillation data with those from cosmology, due to the different parameter spaces in which measurements from these two sets are expressed.

In this article, we discuss a procedure to convert limits on sterile neutrinos between the $(|\Delta m_{41}^2|, \theta_{14}, \theta_{24})$ parameter space of neutrino oscillation physics and the $(m_{\text{eff}}^{\text{sterile}}, \Delta N_{\text{eff}})$ parameter space of cosmology. We use the LASAGNA software package to solve the quantum kinetic equations of neutrinos in the early universe in a 1 + 1 model, allowing us to compare the exclusion regions obtained from Planck data with both allowed regions and exclusion regions from ν_e and $\bar{\nu}_e$ disappearance searches. In a 3 + 1 model, we use a mean momentum approximation to solve the quantum kinetic equations, allowing us to compare the Planck exclusion with allowed regions and exclusion regions corresponding to $\nu_{\mu} \rightarrow \nu_e$ searches. We find that the Planck data strongly excludes the allowed regions from the Neutrino-4, LSND and MiniBooNE experiments, as well as from the gallium

and reactor anomalies. Compared to the Daya Bay exclusion region from ν_e disappearance, Planck is much more constraining above $|\Delta m_{41}^2| \approx 0.1 \text{ eV}^2$ and $m_{\text{eff}}^{\text{sterile}} \approx 0.2 \text{ eV}$, whereas at lower values, Daya Bay provides a more stringent exclusion on θ_{14} . The Planck data provide the strongest exclusion on the $\theta_{\mu e}$ parameter that describes $\nu_\mu \rightarrow \nu_e$ appearance above $\Delta m_{41}^2 \approx 5 \times 10^{-2} \text{ eV}^2$; below this value, the Daya Bay/Bugey/MINOS combination becomes comparable in terms of its exclusion power.

Acknowledgements We are grateful to Thomas Tram (ICG Portsmouth) for help in running the LASAGNA code. We thank Joe Zuntz and Richard Battye (Manchester), and Steen Hannestad (Aarhus) for helpful discussions. This work has been supported by the Science and Technology Facilities Council, part of UK Research and Innovation, the Royal Society, and the European Research Council. Participation of one of the authors (P.G.) has been funded from the European Union's Horizon 2020 research and innovation programme under the Marie Skłodowska-Curie grant agreement no. 752309.

References

1. A. Aguilar *et al.* [LSND Collaboration], Phys. Rev. **D64**, 112007 (2001).
2. A. A. Aguilar-Arevalo *et al.* [MiniBooNE Collaboration], Phys. Rev. Lett. **121**, 221801 (2018).
3. A. P. Serebrov *et al.* [NEUTRINO-4 Collaboration], Pisma Zh. Eksp. Teor. Fiz. **109**, 209 (2019), [JETP Lett. **109**, no.4, 213 (2019)].
4. M. A. Acero, C. Giunti, and M. Laveder, Phys. Rev. **D78**, 073009 (2008).
5. G. Mention, M. Fechner, T. Lasserre, T. A. Mueller, D. Lhuillier, M. Cribier, and A. Letourneau, Phys. Rev. **D83**, 073006 (2011).
6. S. Schael *et al.* [SLD Electroweak Group, DELPHI, ALEPH, SLD, SLD Heavy Flavour Group, OPAL, LEP Electroweak Working Group, L3], Physics Reports **427**, 257 (2006).
7. B. Pontecorvo, Sov. Phys. JETP **26**, 984 (1968).
8. V. N. Gribov and B. Pontecorvo, Phys. Lett. **B28**, 493 (1969).
9. Z. Maki, M. Nakagawa, and S. Sakata, Prog. Theor. Phys. **28**, 870 (1962).
10. N. Aghanim *et al.* [Planck Collaboration] (2018), Planck 2018 results. VI. Cosmological parameters, [1807.06209].
11. P. Adamson *et al.* [MINOS Collaboration], Phys. Rev. Lett. **117**, 151803 (2016).
12. P. Adamson *et al.* [MINOS+ Collaboration], Phys. Rev. Lett. **122**, 091803 (2019).
13. F. P. An *et al.* [Daya Bay Collaboration], Phys. Rev. Lett. **117**, 151802 (2016).
14. P. Adamson *et al.* [Daya Bay and MINOS Collaborations], Phys. Rev. Lett. **117**, 151801 (2016).
15. M. G. Aartsen *et al.* [IceCube Collaboration], Phys. Rev. Lett. **117**, 071801 (2016).
16. M. G. Aartsen *et al.* [IceCube Collaboration], Phys. Rev. **D95**, 112002 (2017).
17. Y. J. Ko *et al.* [NEOS Collaboration], Phys. Rev. Lett. **118**, 121802 (2017).
18. S. Bridle, J. Elvin-Poole, J. J. Evans, S. Fernandez, P. Guzowski, and S. Söldner-Rembold, Phys. Lett. **B764**, 322 (2017).
19. A. M. Knee, D. Contreras, and D. Scott, J. Cosmol. Astropart. Phys. **07**, 039 (2019).
20. I. Esteban, M. Gonzalez-Garcia, M. Maltoni, I. Martinez-Soler, and T. Schwetz, J. High Energy Phys. **01**, 087 (2017).
21. C. Athanassopoulos *et al.* [LSND Collaboration], Nucl. Instrum. Meth. **A388**, 149 (1997).
22. A. Aguilar-Arevalo *et al.* [MiniBooNE Collaboration], Nucl. Instrum. Meth. **A599**, 28 (2009).
23. A. A. Aguilar-Arevalo *et al.* [MiniBooNE Collaboration], Phys. Rev. **D79**, 072002 (2009).
24. https://www-boone.fnal.gov/for_physicists/data_release/, accessed 18-Feb-2020.
25. J. Kopp, P. A. N. Machado, M. Maltoni, and T. Schwetz, J. High Energy Phys. **05**, 050 (2013).
26. F. An *et al.* [Daya Bay Collaboration], Nucl. Instrum. Meth. **A811**, 133 (2016).
27. D. Adey *et al.* [Daya Bay Collaboration], Phys. Rev. Lett. **121**, 241805 (2018).
28. https://wiki.bnl.gov/dayabay/index.php?title=Daya_Bay%27s_Sterile_Neutrino_Results_in_2016, accessed 18-Feb-2020.
29. X. Qian, A. Tan, J. Ling, Y. Nakajima, and C. Zhang, Nucl. Instrum. Meth. **827**, 63 (2016).
30. T. Junk, Nucl. Instrum. Meth. **A434**, 435 (1999).
31. A. L. Read, J. Phys. **G28**, 2693 (2002).
32. B. Achkar *et al.* [Bugey-3 Collaboration], Nucl. Instrum. Meth. **A374**, 164 (1996).
33. B. Achkar *et al.* [Bugey-3 Collaboration], Nucl. Phys. **B434**, 503 (1995).
34. D. G. Michael *et al.* [MINOS Collaboration], Nucl. Instrum. Meth. **A596** (2008).
35. P. Adamson *et al.*, Nucl. Instrum. Meth. **A806**, 279 (2016).
36. P. Adamson *et al.* [MINOS Collaboration], Phys. Rev. Lett. **112**, 191801 (2014).
37. K. Schreckenbach *et al.*, Phys. Lett. **B160**, 325 (1985).
38. P. Vogel, Phys. Rev. **D29**, 1918 (1984).
39. P. Huber, Phys. Rev. **C84**, 024617 (2011), erratum: **85**, 029901 (2012).
40. T. A. Mueller *et al.*, Phys. Rev. **C83**, 054615 (2011).
41. <https://www-numi.fnal.gov/PublicInfo/forscientists.html>, accessed 18-Feb-2020.

-
42. K. N. Abazajian *et al.* [Topical Conveners: K.N. Abazajian, J.E. Carlstrom, A.T. Lee], *Astropart. Phys.* **63**, 66 (2015).
 43. S. Dodelson and L. M. Widrow, *Phys. Rev. Lett.* **72**, 17 (1994).
 44. L. Valenziano *et al.*, *J. Instrum.* **4**, T12006 (2009).
 45. J. M. Lamarre *et al.*, *New Astronomy Reviews* **47**, 1017 (2003).
 46. <http://pla.esac.esa.int/pla/>, accessed 18-Feb-2020.
 47. S. Hannestad, R. S. Hansen, and T. Tram, *J. Cosmol. Astropart. Phys.* **2013**, 032 (2013).
 48. S. Gariazzo, P. F. de Salas, and S. Pastor, *J. Cosmol. Astropart. Phys.* **1907**, 014 (2019).
 49. A. Mirizzi, N. Saviano, G. Miele, and P. D. Serpico, *Phys. Rev.* **D86**, 053009 (2012).
 50. E. Hairer and G. Wanner, *Solving ordinary differential equations II* (Springer, 2006).
 51. B. Ashby, *IntegratorT*, <http://www.unige.ch/~hairer/software.html>, accessed 18-Feb-2020.